Check for updates

Geophysical Research Letters

RESEARCH LETTER
10.1029/2022GL100098

Volume Estimation From Planform Characteristics of Washover Morphology

Eli D. Lazarus[1], Hannah E. Williams[2], and Evan B. Goldstein[3]

[1]Environmental Dynamics Lab, School of Geography and Environmental Science, University of Southampton Highfield Campus, Southampton, UK, [2]Wales Institute for Science and Art, University of Wales Trinity Saint David, Swansea, UK, [3]Department of Geography, Environment, and Sustainability, University of North Carolina at Greensboro, Greensboro, NC, USA

Key Points:

- Washover volume can be estimated from washover area
- Scaling relationships for washover size and shape link measurements from a physical experiment and field examples
- Estimation of washover volume from aerial imagery is a step toward quantifying storm-driven contributions to sediment budgets

Correspondence to:

E. D. Lazarus,
E.D.Lazarus@soton.ac.uk

Citation:

Lazarus, E. D., Williams, H. E., & Goldstein, E. B. (2022). Volume estimation from planform characteristics of washover morphology. *Geophysical Research Letters*, *49*, e2022GL100098. https://doi.org/10.1029/2022GL100098

Received 17 JUN 2022
Accepted 10 NOV 2022

Author Contributions:

Conceptualization: Eli D. Lazarus, Evan B. Goldstein
Data curation: Hannah E. Williams
Formal analysis: Eli D. Lazarus, Hannah E. Williams, Evan B. Goldstein
Funding acquisition: Eli D. Lazarus, Evan B. Goldstein
Investigation: Eli D. Lazarus, Hannah E. Williams, Evan B. Goldstein
Methodology: Eli D. Lazarus, Hannah E. Williams, Evan B. Goldstein
Project Administration: Eli D. Lazarus
Writing – original draft: Eli D. Lazarus, Hannah E. Williams, Evan B. Goldstein

© 2022. The Authors.
This is an open access article under the terms of the Creative Commons Attribution License, which permits use, distribution and reproduction in any medium, provided the original work is properly cited.

Abstract Overwash is the cross-shore transport of water and sediment from a waterbody over the crest of a sand or gravel barrier beach, and washover is the resulting sedimentary deposit. Washover volume, and alongshore patterns of washover distribution, are fundamental components of sediment budgets for low-lying coastal barrier systems. Accurate sediment budgets are essential to forecasting barrier system sustainability under future climate-driven forcing. However, comprehensive surveys of three-dimensional washover morphology are challenging to deliver. Here, we use the results of a physical experiment, analysis of lidar data, and examples of washover characteristics reported in the literature to develop scaling relationships for washover morphometry that demonstrate volume can be reasonably inferred from planform measurements, for washover in natural (non-built) and built barrier settings. Gaining three-dimensional insight into washover deposits from two-dimensional information unlocks the ability to analyze past aerial imagery and estimate contributions from washover flux to sediment budgets for past storms.

Plain Language Summary When a coastal storm drives water up and over the crest of a beach, sediment gets picked up by the flow and deposited behind the beach. That deposit, which might settle among dunes, on a marsh, or on the streets of a neighborhood, is called washover. Knowing the total volume of washover delivered by a storm event helps coastal managers account for the amount of sediment that moves through a beach system over time, known as a sediment budget. An accurate sediment budget provides an indication of environmental functioning and sustainability. However, washover volume is expensive to measure over large spatial scales—so despite its importance to sediment budgets, washover volume often goes unquantified. What if three-dimensional washover volume could be estimated from the two-dimensional shape and size of washover deposits visible in aerial photos? Here, we created washover deposits in a laboratory and compared them to washover in field settings to show that the area of a washover deposit is a good predictor of its volume. This relationship between area and volume unlocks information about past storm deposition captured in aerial photo archives, and enables estimation of washover volume where direct measurement of volume is unavailable or impossible.

1. Introduction

A formative morphodynamic and evolutionary process of low-lying barrier coastlines is overwash (Donnelly et al., 2006; FitzGerald et al., 2008; Leatherman, 1979): the cross-shore transport of water and sediment from a waterbody over the crest of a sand or gravel barrier beach. The resulting sedimentary deposit left by overwash flow is termed washover (Figure 1). Overwash is typical of storm events (Sallenger, 2000), but can occur under any conditions—including fairweather spring tides—in which a waterbody becomes super-elevated relative to the local beach or barrier crest, setting up sufficient hydraulic head to drive cross-shore flow (Donnelly et al., 2006; Fisher & Stauble, 1977; Kobayashi et al., 2010; Matias & Masselink, 2017). Washover volume and alongshore patterns of washover distribution are fundamental components of sediment budgets for barrier systems (Leatherman, 1979; Nienhuis & Lorenzo-Trueba, 2019a, 2019b; Pierce, 1969; Reeves et al., 2022). Sediment budgets are essential to forecasting barrier system sustainability or collapse under future climate-driven forcing (Lorenzo-Trueba & Ashton, 2014).

Despite the importance of washover volume as an empirical constraint, comprehensive surveys of three-dimensional washover morphology are challenging to deliver. Localized field studies of one or a few washover sites are

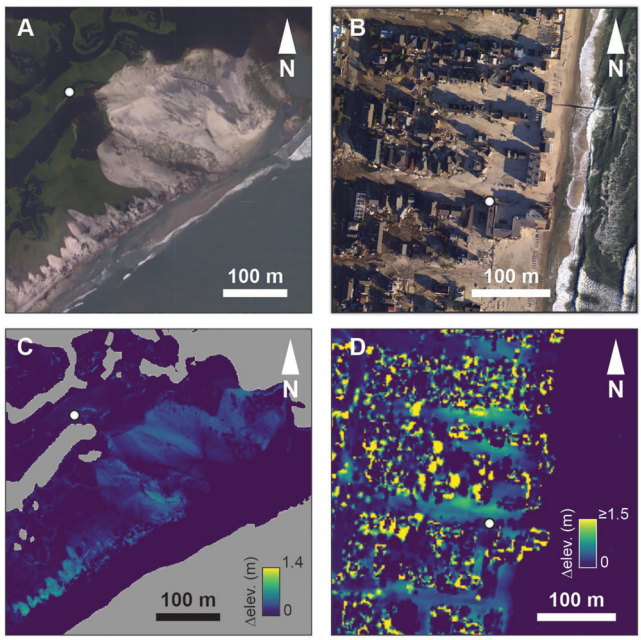

Figure 1. Examples of washover evident in post-storm aerial imagery from (a) natural (non-built) and (b) built settings, and (c and d) the equivalent deposits in lidar-derived, three-dimensional measurement of post-storm topographic change. Gray areas in panel (c) indicate no data. These elevation-difference surfaces were masked to only show positive (depositional) changes in elevation. White dots indicate same location in each image pair: (a, c) Onslow Beach, North Carolina, USA; UTM 18°S 287,034 m°E, 3,824,707 m°N; (b, d) Ortley Beach, New Jersey, USA; UTM 18°S 579,548 m°E, 4423560 m°N. Aerial imagery available from Emergency Response Imagery for (a) Hurricane Florence in 2017 and (b) Hurricane Sandy in 2012 (National Geodetic Survey, 2022). Lidar data available from NOAA Digital Coast (NOAA, 2022): (c) pre-storm: 2017 USACE NCMP Topobathy Lidar digital elevation model (DEM): East Coast; post-storm: 2018 USACE NCMP Post-Florence Topobathy Lidar DEM: Southeast Coast; (d) pre-storm: 2012 USGS EAARL-B Lidar: Pre-Sandy; post-storm: 2012 USGS EAARL-B Lidar: Post-Sandy.

relatively common in the coastal literature, but regional-scale analyses using remote-sensing tools are rare. One reason for that rarity is the availability—or unavailability—of three-dimensional data (i.e., digital elevation models [DEMs]) of sufficiently high spatial and temporal resolution to capture washover occurrence. Post-storm lidar surveys, for example, typically lack an anticipatory pre-storm survey with which to be compared: in some cases pre-storm baselines and post-storm surveys may be years apart (Sherwood et al., 2018; Williams & Rains, 2022)—where lidar is flown at all, let alone with any regularity. High-resolution structure-from-motion photogrammetry is emerging as a promising alternative resource for quantitative post-storm assessment, but for now remains computationally expensive (Sherwood et al., 2018, 2021).

Far more abundant than three-dimensional data sets is post-storm aerial imagery (Figure 1)—particularly along the Atlantic and Gulf Coasts of the USA, thanks to the National Geodetic Survey Emergency Response Imagery program (National Geodetic Survey, 2022). More abundant still is satellite imagery, which may be of sufficient resolution to resolve post-storm washover morphology on barriers around the planet. Washover patterns are readily observable in post-storm aerial imagery, where it is available, motivating exploratory efforts to formalize scaling laws relating three-dimensional washover volume to measured characteristics of the two-dimensional washover planform (Lazarus, 2016; Overbeck et al., 2015; Rogers et al., 2015). However, scaling relationships derived from field settings have attempted to link washover volume only to cross-shore intrusion length (Overbeck et al., 2015; Rogers et al., 2015). This transect-oriented vantage aligns with way washover volume is commonly reported—not as the total volume of the whole deposit, but normalized as the volume per meter of cross-shore intrusion length ($m^3\ m^{-1}$), which is readily converted into a flux. Others have noted (Carruthers et al., 2013) that this normalizing convention is inconsistently applied: some studies normalize washover volume by alongshore extent, which has the same units. Washover volume (normalized or not) as a function of intrusion length tends to be a noisy relationship, dominated by scatter. Results of a physical experiment indicated that washover area could be a strong predictor of volume (Lazarus, 2016); although those experimental deposits at the $\sim 10^{-1}$ m scale showed geometric and kinematic similarity to deposits in field settings (Paola et al., 2009), a relationship between volume and area was not tested for field examples (Lazarus, 2016).

Furthermore, empirical scaling relationships for washover are complicated by the presence of built environments (Lazarus et al., 2021; Rogers et al., 2015), and by related human interventions in the intrinsic sediment pathways of barrier systems. In the USA, for example, many barrier systems are now intensively developed (Aldabet et al., 2022). Scaling relationships for planform characteristics of washover into built settings break at high built fractions (total building footprint per unit area), such that washover in built and natural (non-built) settings become quantitatively distinct (Lazarus et al., 2021). Numerical models of barrier morphodynamics—coupling hydrodynamic forcing, sediment transport, and three-dimensional morphology—might produce realistic washover dynamics in natural barrier settings but perform poorly for built settings (Nienhuis et al., 2021). Initial empirical work has suggested that built environments may impart a scaling effect on washover volume (Rogers et al., 2015), but those findings—from cross-shore transects through a lidar-derived surface—only relate washover volume to intrusion length, and do not consider whole-deposit morphology. Nor can lidar be relied upon to record washover into built settings, because sediment (and other storm-driven debris) deposited on streets and roads is quickly cleared with earth-moving equipment to maintain emergency services (Lazarus et al., 2021; Nordstrom, 2004)—sometimes while deposition is actively underway (Lazarus & Goldstein, 2019). Aerial imagery may thus comprise the best record—and in most cases the only record—of washover deposition across natural and built barrier settings alike.

19448007, 2022, 22, Downloaded from https://agupubs.onlinelibrary.wiley.com/doi/10.1029/2022GL100098, Wiley Online Library on [13/11/2023]. See the Terms and Conditions (https://onlinelibrary.wiley.com/terms-and-conditions) on Wiley Online Library for rules of use; OA articles are governed by the applicable Creative Commons License

19448007, 2022, 22, Downloaded from https://agupubs.onlinelibrary.wiley.com/doi/10.1029/2022GL100098, Wiley Online Library on [13/11/2023]. See the Terms and Conditions (https://onlinelibrary.wiley.com/terms-and-conditions) on Wiley Online Library for rules of use; OA articles are governed by the applicable Creative Commons License

The circumstances of this data-dependent context prompts a basic question: What if three-dimensional washover volume could be estimated accurately from two-dimensional planform morphometry, in a variety of settings and at a range of spatial scales? How might that transform the utility of aerial imagery to enable more exhaustive empirical analysis of washover characteristics and patterns? Gaining three-dimensional insight into washover deposits from two-dimensional information unlocks the ability to analyze past aerial (and potentially satellite) imagery and reconstruct subaerial sand budgets for past storms—specifically, estimation of washover flux, a key constraint for modeling, understanding, and managing barrier system sustainability (Ashton & Lorenzo-Trueba, 2018; Lorenzo-Trueba & Ashton, 2014; McNamara & Werner, 2008a, 2008b; Miselis & Lorenzo-Trueba, 2017; Nienhuis & Lorenzo-Trueba, 2019a; Nienhuis et al., 2021; Passeri et al., 2020; Reeves et al., 2022). Here, we use the results of a physical experiment, analysis of lidar data, and examples of washover characteristics reported in the literature to develop scaling relationships for washover morphometry that demonstrate volume can be reasonably inferred from planform measurements in natural (non-built) and built barrier settings.

2. Methods

2.1. Physical Experiment

To generate a data set of model washover morphology for comparison against remotely sensed observations from field settings, we conducted a physical experiment that examined under controlled conditions how washover morphology manifests in non-built and built settings under the same forcing (Figure 2). This experiment complements recent laboratory-based explorations of barrier dynamics, some of which have focused on cross-shore processes in gravel systems (i.e., BARDEX: Masselink et al., 2013; J. J. Williams et al., 2012), and others on morphodynamics in atoll motu systems (Tuck, Ford, et al., 2019; Tuck, Kench, et al., 2019), subaerial delta fronts (Rodgers & Paola, 2021), and spatially extended barrier settings (Lazarus, 2016; Lazarus & Armstrong, 2015; Lazarus et al., 2020). (For a summary of early laboratory studies of overwash, see Donnelly et al., 2006.) Most physical models of overwash morphology are constructed as a shore-orthogonal barrier cross-section (Donnelly et al., 2006; Masselink et al., 2013; J. J. Williams et al., 2012), which emphasizes topographic changes in the beach and barrier profile but neglects lateral effects (e.g., whole-deposit formation, sharing and capture of overwash flow), whether at the scale of a single washover deposit (Rodriguez et al., 2020; Williams, 2015) or across many deposits in series (Lazarus, 2016; Lazarus & Armstrong, 2015; Lazarus et al., 2020; Rodgers & Paola, 2021). Here, we followed the premise of a previous physical experiment—smaller in scale by an order of magnitude—by Lazarus (2016), which produced barrier overwash morphology arrayed along a spatially extended, topographically uniform, non-built domain. We used an experimental design that is likewise spatially extended in the alongshore dimension, thus generating in each trial multiple washover features ($n \sim 10^1$) and a distribution of morphometric characteristics even under constant forcing.

This experiment took place in the Total Environment Simulator (TES) at the University of Hull (UK). The TES is a 6 × 10 m modular basin, fully enclosed on three sides with an outlet fully spanning one end of the flume to allow recirculation of water. Following the basic experimental design described by Lazarus (2016), we constructed a topographically uniform, low barrier (0.05 m height × 1 m cross-shore width × 10 m alongshore length) of sorted, medium sand ($D_{50} \sim 0.25$–0.5 mm) spanning the long dimension of the flume (Figures 2a–2c). Barrier uniformity and reproducibility was achieved by mounting a plywood template of the cross-shore profile to an overhead gantry, and running the template along the length of a loosely shaped barrier. The combination of a spatially extended alongshore dimension and low barrier elevation facilitates, in a given trial, the formation of many overwash sites and corresponding washover deposits (order $n \sim 10^1$) arrayed along the barrier. Moreover, a topographically uniform initial barrier with such a stretched aspect ratio—much as coastal barriers in the field are characteristically elongate in their alongshore dimension (Mulhern et al., 2017)—creates space for alongshore patterning of washover morphology (Lazarus, 2016; Lazarus & Armstrong, 2015; Lazarus et al., 2020).

To drive the overwash process, one side of the barrier (the "ocean" side) was gradually filled as a reservoir; discharge into the reservoir was held constant, and inflow was baffled using a box of cobbles. Overwash flow and washover deposition began once the water level in the reservoir exceeded the height of the barrier crest. The receiving side of the barrier (the "back-barrier floodplain" side) was left dry, and overwash flow was allowed to drain away. A trial ended when sediment transport had effectively ceased (typically ~20–25 min). The back-barrier floodplain was either left baer, to represent a non-built barrier setting, or was configured with blocks of bricks

19448007, 2022, 22, Downloaded from https://agupubs.onlinelibrary.wiley.com/doi/10.1029/2022GL100098, Wiley Online Library on [13/11/2023]. See the Terms and Conditions (https://onlinelibrary.wiley.com/terms-and-conditions) on Wiley Online Library for rules of use; OA articles are governed by the applicable Creative Commons License

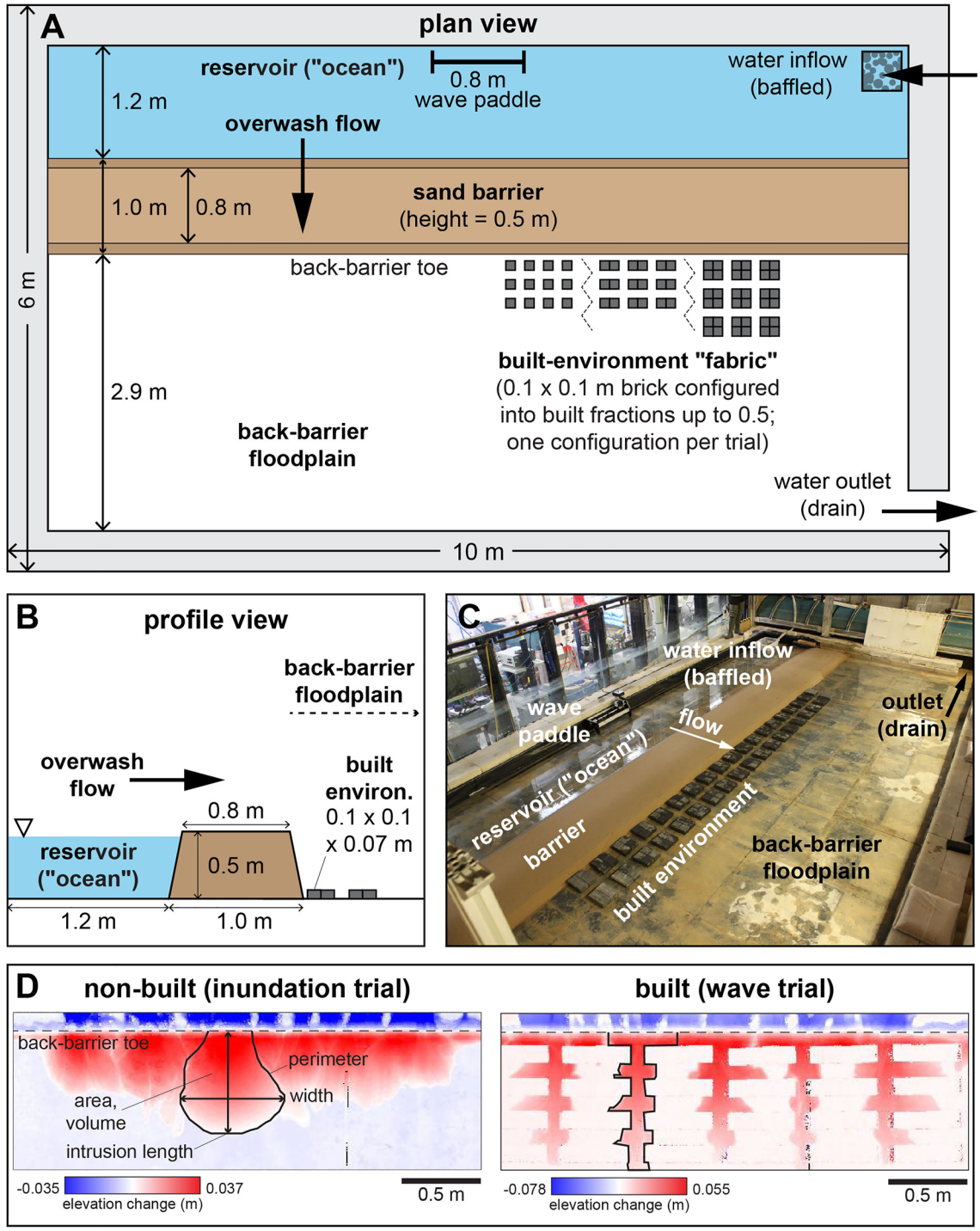

Figure 2. Experimental set-up in the Total Environment Simulator (TES) and representative resulting morphologies. Experimental schematic in (a) plan and (b) profile view; (c) oblique photo from inside the TES of a pre-trial set-up. (d) Examples of differenced topographic scans (final minus initial conditions) and resulting washover morphology from a non-built trial with inundation forcing (left) and built trial with wave-driven forcing (right).

to represent a built setting. Brick units were gridded into different patterns to represent a range of built fractions (Lazarus et al., 2021), taken as the total footprint area of brick units relative to the total area built (including the open space between brick blocks—see Figure 2a).

19448007, 2022, 22, Downloaded from https://agupubs.onlinelibrary.wiley.com/doi/10.1029/2022GL100098, Wiley Online Library on [13/11/2023]. See the Terms and Conditions (https://onlinelibrary.wiley.com/terms-and-conditions) on Wiley Online Library for rules of use; OA articles are governed by the applicable Creative Commons License

We tested two forcing regimes: one in which overwash flow is driven by still-water levels above the barrier elevation, mimicking barrier inundation (Lazarus, 2016); and one in which overwash flow is driven by wave overtopping (Sallenger, 2000). For inundation, inflow into the ocean reservoir was continuous (2.9 Ls^{-1}) and water allowed to flow freely over the barrier. For wave-driven forcing, the seaward reservoir was filled with water to the height of the barrier crest, and then a small wave paddle (Emriver EM2 wave paddle; ~1.1 s period; ~0.01 m wave amplitude) was used to push water over the barrier. The wave paddle was able to drive overwash across approximately 4 m of the barrier at a time; when sediment transport had effectively ceased in one half, the trial was paused, the paddle shifted to face the unworked half of the barrier, and the trail restarted.

The full barrier was scanned before and after a trial (drained) using an overhead-mounted terrestrial laser scanner to generate DEMs (resolution to within ~1.5 mm). The raw point-clouds were processed using the inbuilt software of the FARO laser scanner mounted in the TES. Taking the difference between the resulting DEMs to emphasize patterns of accretion, we manually identified and digitized 501 individual washover deposits and measured their morphometric characteristics (Figure 2d). Identification and digitization of the experimental deposits was done by the same person. Deposits evident in the elevation-difference surfaces were checked against overhead imagery. Some washover deposits, as delineated, may overlap with neighboring deposits. Another person might have delineated some of the deposits differently—decisions labeling washover are known to vary between people (Goldstein et al., 2021). These differences may lead to subtle differences in measured characteristics, but considering the number of washover deposits collectively delineated and measured by many different workers—in this analysis, and in related literature—overall scaling relationships from large and/or aggregated data sets appear insensitive to detailed interpretations by an individual.

We conducted 22 trials in total: 7 inundation regime (3 non-built, 4 built) and 15 wave regime (2 non-built, 13 built). Collectively, these produced 182 inundation-driven and 319 wave-driven deposits, 143 in non-built and 358 in built conditions. We did not investigate the potential influence of other parameters contributing to the experimental built environment (e.g., number of back-barrier rows, spacing around bricks, etc.). Detailed conditions for each experimental trial, along with all of the experimental data, are available from H. E. Williams et al. (2022).

2.2. Lidar Analysis

We measured washover morphometry, including volume, for 148 deposits in natural (non-built) and built settings along the barrier coastline of New Jersey, USA, by taking the difference between lidar-derived DEMs bracketing Hurricane Sandy (2012). We also collated 35 measurements of washover morphometry, including volume, reported in the literature by six different studies, sampling different storm events in different non-built barrier settings (Carruthers et al., 2013; Hansen et al., 2021; Rodriguez et al., 2020; Williams, 2015; Williams & Rains, 2022), including a carbonate system (Jamison-Todd et al., 2020). Lidar surfaces were downloaded from the NOAA Digital Coast Data Access Viewer (NOAA, 2022). Geospatial analysis was done in QGIS version 3.22.5. We masked both the pre- and post-storm surfaces to isolate only positive elevations (>0 m relative to the North American Vertical Datum of 1988 [GEOID12A model], in which the original data are rendered; this masking is inevitably a simplified representation of the subaerial barrier, but also works around artifactual "holes" in the lidar layers) and subtracted the pre-storm surface from the post-storm surface to calculate the difference between them. We then retained only the positive differences in the resulting surface to isolate sites of sediment deposition. We manually digitized the perimeters of depositional forms we interpreted as washover, corroborated by aerial imagery (National Geodetic Survey, 2022).

Basic geometric characteristics (perimeter, area) were taken directly from the washover polygons; washover length and width were taken from oriented minimum bounding boxes around each polygon (calculated with an inbuilt tool in QGIS that aligns a minimum bounding box with the principal axis of the inscribed polygon). Volume for each washover polygon was measured using the Volume Calculation Tool (version 0.4) plugin for QGIS (REDcatch GmbH, 2022). In built settings, each washover deposit was associated with a locally estimated built fraction (Lazarus et al., 2021). Elements of the built environment (i.e., buildings) were isolated by creating a binary mask of the pre-storm surface, such that all elevations ≥5 m were set to a value = 1, and all elevations <5 m set to zero. Minimum enclosing circles were drawn around each washover polygon, and the total built area (masked value = 1) within each circle summed using the QGIS Zonal Statistics tool. Here, local built fraction is the total built area within a minimum enclosing circle divided by the area of that circle.

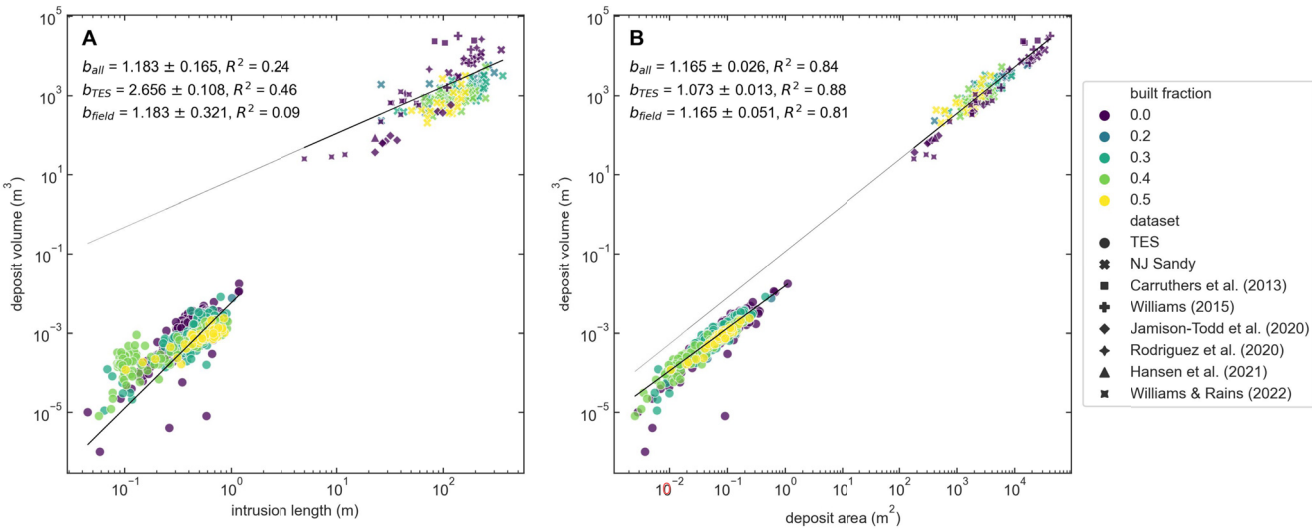

Figure 3. Scaling relationships for washover volume as a function of (a) length and (b) area, spanning the physical experimental results from the Total Environment Simulator and washover deposits in the field from lidar analysis (n = 8 non-built, 140 built) and examples reported in the literature (n = 35, all non-built). Note that for all symbols, color indicates built fraction. These results suggest that the best planform predictor of washover volume is area. Nonlinear regressions of the form $y = ax^b$ were performed in linear space to avoid log-transformation bias (c.f. Ferguson, 1986); results are plotted in log-log space. Extended gray regression line (with scaling exponent b_{all}) in each panel spans both the experimental (cluster at lower left; black regression line with scaling exponent b_{TES}) and field deposits (upper right; black regression line with scaling exponent b_{field}).

There is insufficient contextual data regarding the *in situ* conditions under which these washover deposits formed to differentiate between inundation and wave-driven forcing—and in field settings, washover deposits may reflect a combination of both. The geospatial data layers that we created, along with the resulting washover morphometry and references to the lidar surveys underpinning these data, are available from Lazarus et al. (2022a, 2022b).

3. Results and Discussion

Drawing on collated measurements of experimental and field examples of washover morphology, we formalize scaling relationships for deposit volume as a function of two primary planform characteristics: intrusion length (Figure 3a) and deposit area (Figure 3b). Of these two relationships, volume as a function of area reflects less variability in its distribution. Normalizing washover volume by intrusion length—and then plotting as a function of intrusion length, per convention—does not deliver as clear a scaling relationship because the three-dimensionality of the deposit gets negated: a transect might slice through a deposit near its lateral margin, and so return an anomalously low volume, or slice a deposit through its thickest region and reflect the maximum volume. Given that washover deposits appear to exhibit allometric growth (Lazarus et al., 2020), such that dimensions of washover morphology are not only scaled relative to each other but *change* relative to each other in an organized way, our results indicate the importance of whole-deposit considerations in estimations of washover flux.

Unlike other scaling relationships between washover characteristics, such as any involving perimeter (Lazarus et al., 2021), washover volume as a function of area appears generally insensitive to built fraction. Our finding differs from previous empirical work that suggested built environments do impart a scaling effect on washover volume (Rogers et al., 2015). This is not to say that high built fraction has no effect on washover magnitude: a barrier with a high built fraction ipso facto has less accommodation space in which any deposition can occur. Where built fraction is high—and where buildings are not on pilings or otherwise elevated—sediment can only go down streets and between structures. Yet while the planform shape of a washover deposit may become highly distorted, we find that the scaling relationship between area and volume is preserved. This relative insensitivity to built fraction suggests that area, specifically, may serve as a powerful predictor of washover volume in a wide variety of barrier environments. That is, rather than requiring different scaling relationships across a range of built fractions, volume as a function of area describes a single scaling relationship for all built fractions.

19448007, 2022, 22, Downloaded from https://agupubs.onlinelibrary.wiley.com/doi/10.1029/2022GL100098, Wiley Online Library on [13/11/2023]. See the Terms and Conditions (https://onlinelibrary.wiley.com/terms-and-conditions) on Wiley Online Library for rules of use; OA articles are governed by the applicable Creative Commons License

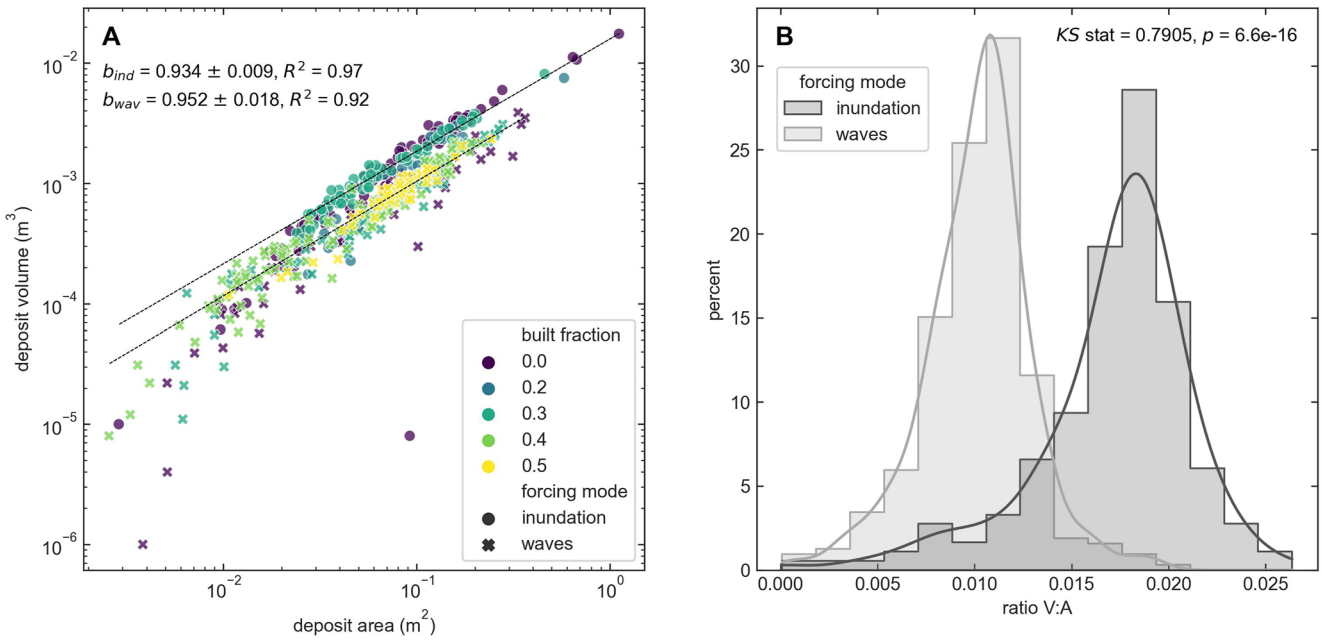

Figure 4. (a) Scaling relationship for washover volume as a function of area, from the Total Environment Simulator experimental results. Nonlinear regressions of the form $y = ax^b$ were performed in linear space to avoid log-transformation bias (c.f. Ferguson, 1986); results are plotted in log space. Numbers of deposits in each (binned) built fraction: n = 182 (bf 0.0), 26 (0.2), 141 (0.3), 141 (0.4), and 51 (0.5). Regressions for inundation and wave-driven forcing return approximately equivalent scaling exponents and are only shifted in log-log space by their coefficients, reflecting that panel (b) inundation forcing in the experiment yielded washover with greater volume per area than their wave-driven counterparts (n = 182 inundation-driven, 319 wave-driven). A two-tailed Kolmogorov-Smirnoff test of the distributions in panel (b) confirms that the experimental inundation- and wave-driven washover deposits represent statistically distinct distributions. These results suggest a scaling continuum between "overwash" and "inundation" regimes of the Sallenger (2000) storm impact scale for barriers.

Overwash processes and washover formation are notoriously difficult to observe and record *in situ* (Engelstad et al., 2017, 2018; Leatherman & Zaremba, 1987; Matias & Masselink, 2017), and as long as three-dimensional surveys of post-storm impacts remain sparse, physical experiments can inform and corroborate numerical modeling of storm impacts on barrier systems (e.g., McCall et al., 2010; Miselis & Lorenzo-Trueba, 2017; Nienhuis et al., 2021; Passeri et al., 2020; Rogers et al., 2015; Smallegan & Irish, 2017) and motivate testable hypotheses regarding future barrier dynamics. Something we were uniquely able to observe in the experiment is a marked morphological distinction between inundation- and wave-driven washover (Figure 4)—the two forcing regimes at the upper end of the Sallenger storm-impact scale (Sallenger, 2000). In the scaling relationship for volume as a function of area, the scaling exponents for the two forcing regimes are effectively indistinguishable (Figure 4a), but inundation-driven washover consistently yielded more volume per unit area than wave-driven washover. A two-tailed Kolmogorov-Smirnoff test confirms that the experimental inundation- and wave-driven washover deposits represent statistically distinct distributions (Figure 4b). Inundation-driven deposits in the experimental trials were perhaps thicker than their wave-driven counterparts because cross-shore overwash flow under inundation forcing was comparatively deeper and more sustained, capable of affecting greater sediment transport. The generic barrier system in this physical experiment was not supply-limited: there was more sediment available in the barrier than the forcings applied could transport. Future work could quantify how inundation and wave-driven forcing regimes shape washover morphology in field settings, and/or test different conditions of sediment availability. For example, a supply-limited system might produce the opposite result, wherein volume is retained in wave-driven washover but lost with inundation and potential breaching (Nienhuis et al., 2021). A broader avenue of future work might explicitly link dynamic allometry in washover to overwash hydrodynamics and mechanics of deposition, and thus address the gap, typical of empirical scaling relationships (Mackin, 1963), between the observation of scaling patterns in washover morphology and mechanistic explanations for them.

19448007, 2022, 22, Downloaded from https://agupubs.onlinelibrary.wiley.com/doi/10.1029/2022GL100098, Wiley Online Library on [13/11/2023]. See the Terms and Conditions (https://onlinelibrary.wiley.com/terms-and-conditions) on Wiley Online Library for rules of use; OA articles are governed by the applicable Creative Commons License

19448007, 2022, 22, Downloaded from https://agupubs.onlinelibrary.wiley.com/doi/10.1029/2022GL100098, Wiley Online Library on [13/11/2023]. See the Terms and Conditions (https://onlinelibrary.wiley.com/terms-and-conditions) on Wiley Online Library for rules of use; OA articles are governed by the applicable Creative Commons License

4. Implications

Our results suggest promising potential for using scaling relationships to estimate from remotely sensed imagery washover contributions to barrier system sediment budgets, in any barrier setting. Estimation of washover bulk volume from measurement of washover planforms evident in remotely sensed imagery could inform post-storm clean-up operations and quantify impacts to critical infrastructure, such as road networks (Aldabet et al., 2022; Kasmalkar et al., 2021; Velasquez-Montoya et al., 2021)—information relevant to planners and authorities responsible for emergency management, among other essential services. Paired comparisons between non-built and built barrier settings are a means of understanding how the latter function as geomorphic systems in their own right (Nordstrom, 1994), and how the two types of settings may evolve in divergent ways with changes in climate-driven forcing. Detailed qualitative descriptions of washover into built settings (Bush, 1991; Hall & Halsey, 1991; Nordstrom, 1994, 2004) are gradually being expanded upon with quantitative observations, particularly in the wake of hurricanes along the US Atlantic and Gulf coastlines (Lazarus et al., 2021; Morton & Payne, 1985; Morton & Sallenger, 2003; Rogers et al., 2015). How washover deposition into built environments affects and informs the evolution of human-altered barrier systems is largely unknown, as is how washover deposition into built settings should inform sediment budgets for predictive numerical models. Where and how much washover sediment gets redistributed by road crews during emergency clean-up operations remains unclear and unquantified (Lazarus & Goldstein, 2019). Washover sediment that gets plowed back to the upper beach profile and/or fronting dune may temporarily recharge the seaward face of the barrier at the expense of building up elevation relative to sea level (c.f. Miselis & Lorenzo-Trueba, 2017). Any washover sediment that does reach the back-barrier ultimately contributes to barrier transgression and persistence, but on more immediate time scales will likely appear to exacerbate shoreline erosion. Estimated subaerial washover flux for past storms, using historical imagery, could indicate whether storm-driven sediment budgets have changed over time, especially in settings where built environments have expanded.

As post-storm observational data sets rapidly expand (National Geodetic Survey, 2022), so do opportunities to measure and investigate washover expression and morphology in its surprising variety (Goldstein et al., 2020, 2021; Morton & Payne, 1985; Morton & Sallenger, 2003; Williams, 2015). Motivated by scaling relationships like those we report here, future work should compare barrier washover patterns from as many different settings and contexts as possible (Almeida et al., 2012; Carrasco et al., 2012; Ceia et al., 2010; Garcia et al., 2010; Kombiadou et al., 2019; Matias et al., 2008; Mulhern et al., 2017; Stutz & Pilkey, 2011)—not only to generate a more comprehensive distribution of washover morphometrics, but also to identify where scaling relationships break, and under what conditions. Future experiments—physical and numerical—and more inclusive empirical observation may test and refine the scaling relationships presented here (e.g., with direct examination of antecedent topography, grain size, storm frequency, influence of structure-elevating pilings, etc.), and further clarify fundamental controls on washover volume.

Acknowledgments
The authors thank Stuart McLelland, Brendan Murphy, Xuxu Wu, and Daniel Parsons for access to, and help with, the Total Environment Simulator for these experimental trials at the University of Hull. Gerd Masselink, Charlie Thompson, Pieter Roos, Henk Schuttelaars, and Ana Matias contributed helpful discussions regarding an early concept for this work. The authors thank Chris Sherwood and Jin-Si Over for constructive comments, and also the editors, Jennifer Miselis, and an anonymous reviewer. The authors gratefully acknowledge financial support from The Leverhulme Trust (RPG-2018-282, to EDL and EBG), and an Early-Career Research Fellowship from the Gulf Research Program of the National Academies of Sciences, Engineering, and Medicine (to EBG). The content is solely the responsibility of the authors and does not necessarily represent the official views of the Gulf Research Program of the National Academies of Sciences, Engineering, and Medicine.

Data Availability Statement

All data sets and analytical code used in this study are publicly available from the cited sources listed in the manuscript text: experimental data sets (H. E. Williams et al., 2022), geospatial data layers (Lazarus et al., 2022b), and our analysis code (Lazarus et al., 2022a). This manuscript also relies on open data, specifically lidar data sets via the NOAA Digital Coast Data Access Viewer (https://coast.noaa.gov/dataviewer/#/lidar/search/) detailed in the description of Figure 1.

References

Aldabet, S., Goldstein, E. B., & Lazarus, E. D. (2022). Thresholds in road network functioning on US Atlantic and Gulf barrier islands. *Earth's Future*, *10*(5), e2021EF002581. https://doi.org/10.1029/2021EF002581

Almeida, L. P., Vousdoukas, M. V., Ferreira, Ó., Rodrigues, B. A., & Matias, A. (2012). Thresholds for storm impacts on an exposed sandy coastal area in southern Portugal. *Geomorphology*, *143*, 3–12. https://doi.org/10.1016/j.geomorph.2011.04.047

Ashton, A. D., & Lorenzo-Trueba, J. (2018). Morphodynamics of barrier response to sea-level rise. In L. Moore & A. B. Murray (Eds.), *Barrier dynamics and response to changing climate* (pp. 277–304). Springer. https://doi.org/10.1007/978-3-319-68086-6_9

Bush, D. M. (1991). Impact of Hurricane Hugo on the rocky coast of Puerto Rico. *Journal of Coastal Research*, *SI8*, 49–67. Retrieved from https://www.jstor.org/stable/25735407

Carrasco, A. R., Ferreira, Ó., Matias, A., & Freire, P. (2012). Natural and human-induced coastal dynamics at a back-barrier beach. *Geomorphology*, *159*, 30–36. https://doi.org/10.1016/j.geomorph.2012.03.001

Carruthers, E. A., Lane, D. P., Evans, R. L., Donnelly, J. P., & Ashton, A. D. (2013). Quantifying overwash flux in barrier systems: An example from Martha's Vineyard, Massachusetts, USA. *Marine Geology*, *343*, 15–28. https://doi.org/10.1016/j.margeo.2013.05.013

Ceia, F. R., Patrício, J., Marques, J. C., & Dias, J. A. (2010). Coastal vulnerability in barrier islands: The high risk areas of the Ria Formosa (Portugal) system. *Ocean & Coastal Management*, *53*(8), 478–486. https://doi.org/10.1016/j.ocecoaman.2010.06.004

Donnelly, C., Kraus, N., & Larson, M. (2006). State of knowledge on measurement and modeling of coastal overwash. *Journal of Coastal Research*, *22*(4), 965–991. https://doi.org/10.2112/04-0431.1

Engelstad, A., Ruessink, B. G., Hoekstra, P., & van der Vegt, M. (2018). Sand suspension and transport during inundation of a Dutch barrier island. *Journal of Geophysical Research: Earth Surface*, *123*(12), 3292–3307. https://doi.org/10.1029/2018JF004736

Engelstad, A., Ruessink, B. G., Wesselman, D., Hoekstra, P., Oost, A., & van der Vegt, M. (2017). Observations of waves and currents during barrier island inundation. *Journal of Geophysical Research: Oceans*, *122*(4), 3152–3169. https://doi.org/10.1002/2016JC012545

Ferguson, R. I. (1986). River loads underestimated by rating curves. *Water Resources Research*, *22*(1), 74–76. https://doi.org/10.1029/wr022i001p00074

Fisher, J. S., & Stauble, D. K. (1977). Impact of Hurricane Belle on Assateague Island washover. *Geology*, *5*(12), 765–768. https://doi.org/10.1130/0091-7613(1977)5<765:IOHBOA>2.0.CO;2

FitzGerald, D. M., Fenster, M. S., Argow, B. A., & Buynevich, I. V. (2008). Coastal impacts due to sea-level rise. *Annual Review of Earth and Planetary Sciences*, *36*(1), 601–647. https://doi.org/10.1146/annurev.earth.35.031306.140139

Garcia, T., Ferreira, Ó., Matias, A., & Dias, J. A. (2010). Overwash vulnerability assessment based on long-term washover evolution. *Natural Hazards*, *54*(2), 225–244. https://doi.org/10.1007/s11069-009-9463-3

Goldstein, E. B., Buscombe, D., Lazarus, E. D., Mohanty, S. D., Rafique, S. N., Anarde, K. A., et al. (2021). Labeling poststorm coastal imagery for machine learning: Measurement of interrater agreement. *Earth and Space Science*, *8*(9), e2021EA001896. https://doi.org/10.1029/2021EA001896

Goldstein, E. B., Mohanty, S. D., Rafique, S. N., & Valentine, J. (2020). An active learning pipeline to detect hurricane washover in post-storm aerial images. *AI for Earth sciences workshop at NeurIPS* 2020. https://doi.org/10.31223/X5JW23

Hall, M. J., & Halsey, S. D. (1991). Comparison of overwash penetration from Huricane Hugo and pre-storm erosion rates for Myrtle Beach and North Myrtle Beach, South Carolina, USA. *Journal of Coastal Research*, *SI8*, 229–235. Retrieved from https://www.jstor.org/stable/25735417

Hansen, L. Ø., Ernstsen, V. B., Clemmensen, L. B., Al-Hamdani, Z., & Kroon, A. (2021). A method for estimating sediment budgets of washover deposits using digital terrain models. *Earth Surface Processes and Landforms*, *46*(4), 804–821. https://doi.org/10.1002/esp.5066

Jamison-Todd, S., Stein, N., Overeem, I., Khalid, A., & Trower, E. J. (2020). Hurricane deposits on carbonate platforms: A case study of hurricane Irma deposits on little Ambergris Cay, Turks and Caicos Islands. *Journal of Geophysical Research: Earth Surface*, *125*(8), e2020JF005597. https://doi.org/10.1029/2020JF005597

Kasmalkar, I. G., Serafin, K. A., & Suckale, J. (2021). Integrating urban traffic models with coastal flood maps to quantify the resilience of traffic systems to episodic coastal flooding. *MethodsX*, *8*, 101483. https://doi.org/10.1016/j.mex.2021.101483

Kobayashi, N., Farhadzadeh, A., Melby, J., Johnson, B., & Gravens, M. (2010). Wave overtopping of levees and overwash of dunes. *Journal of Coastal Research*, *26*(5), 888–900. https://doi.org/10.2112/JCOASTRES-D-09-00034.1

Kombiadou, K., Matias, A., Ferreira, Ó., Carrasco, A. R., Costas, S., & Plomaritis, T. (2019). Impacts of human interventions on the evolution of the Ria Formosa barrier island system (S. Portugal). *Geomorphology*, *343*, 129–144. https://doi.org/10.1016/j.geomorph.2019.07.006

Lazarus, E. D. (2016). Scaling laws for coastal overwash morphology. *Geophysical Research Letters*, *43*(23), 113–119. https://doi.org/10.1002/2016GL071213

Lazarus, E. D., & Armstrong, S. (2015). Self-organized pattern formation in coastal barrier washover deposits. *Geology*, *43*(4), 363–366. https://doi.org/10.1130/G36329.1

Lazarus, E. D., Davenport, K. L., & Matias, A. (2020). Dynamic allometry in coastal overwash morphology. *Earth Surface Dynamics*, *8*(1), 37–50. https://doi.org/10.5194/esurf-8-37-2020

Lazarus, E. D., & Goldstein, E. B. (2019). Is there a bulldozer in your model? *Journal of Geophysical Research: Earth Surface*, *124*(3), 696–699. https://doi.org/10.1029/2018JF004957

Lazarus, E. D., Goldstein, E. B., Taylor, L. A., & Williams, H. E. (2021). Comparing patterns of hurricane washover into built and unbuilt environments. *Earth's Future*, *9*(3), e2020EF001818. https://doi.org/10.1029/2020EF001818

Lazarus, E. D., Goldstein, E. B., & Williams, H. E. (2022a). Code for 'Volume estimation from planform characteristics of washover morphology [Dataset]. Zenodo. https://doi.org/10.5281/zenodo.6641396

Lazarus, E. D., Goldstein, E. B., & Williams, H. E. (2022b). Washover morphometry: Lidar-derived and reported in literature [Dataset]. Zenodo. https://doi.org/10.5281/zenodo.7075323

Leatherman, S. P. (1979). Migration of Assateague Island, Maryland, by inlet and overwash processes. *Geology*, *7*(2), 104–107. https://doi.org/10.1130/0091-7613(1979)7<104:MOAIMB>2.0.CO;2

Leatherman, S. P., & Zaremba, R. E. (1987). Overwash and aeolian processes on a U.S. northeast coast barrier. *Sedimentary Geology*, *52*(3–4), 183–206. https://doi.org/10.1016/0037-0738(87)90061-3

Lorenzo-Trueba, J., & Ashton, A. D. (2014). Rollover, drowning, and discontinuous retreat: Distinct modes of barrier response to sea-level rise arising from a simple morphodynamic model. *Journal of Geophysical Research: Earth Surface*, *119*(4), 779–801. https://doi.org/10.1002/2013JF002941

Mackin, J. H. (1963). Rational and empirical methods of investigation in geology. In C. C. Albritton & C. Freeman (Eds.), *The fabric of geology* (pp. 135–163).

Masselink, G., Turner, I., Conley, D., Ruessink, G., Matias, A., Thompson, C., et al. (2013). BARDEX II: Bringing the beach to the laboratory–again. *Journal of Coastal Research*, *65*(10065), 1545–1550. https://doi.org/10.2112/SI65-261.1

Matias, A., Ferreira, Ó., Vila-Concejo, A., Garcia, T., & Dias, J. A. (2008). Classification of washover dynamics in barrier islands. *Geomorphology*, *97*(3–4), 655–674. https://doi.org/10.1016/j.geomorph.2007.09.010

Matias, A., & Masselink, G. (2017). Overwash processes: Lessons from fieldwork and laboratory experiments. In P. Ciavola & G. Coco (Eds.), *Coastal storms* (pp. 175–194). https://doi.org/10.1002/9781118937099.ch9

McCall, R. T., De Vries, J. V. T., Plant, N. G., Van Dongeren, A. R., Roelvink, J. A., Thompson, D. M., & Reniers, A. J. H. M. (2010). Two-dimensional time dependent hurricane overwash and erosion modeling at Santa Rosa Island. *Coastal Engineering*, *57*(7), 668–683. https://doi.org/10.1016/j.coastaleng.2010.02.006

McNamara, D. E., & Werner, B. T. (2008a). Coupled barrier island–resort model: 1. Emergent instabilities induced by strong human-landscape interactions. *Journal of Geophysical Research*, *113*(F1), F01016. https://doi.org/10.1029/2007JF000840

McNamara, D. E., & Werner, B. T. (2008b). Coupled barrier island–resort model: 2. Tests and predictions along ocean city and Assateague Island national seashore, Maryland. *Journal of Geophysical Research*, *113*(F1), F01017. https://doi.org/10.1029/2007JF000841

19448007, 2022, 22, Downloaded from https://agupubs.onlinelibrary.wiley.com/doi/10.1029/2022GL100098, Wiley Online Library on [13/11/2023]. See the Terms and Conditions (https://onlinelibrary.wiley.com/terms-and-conditions) on Wiley Online Library for rules of use; OA articles are governed by the applicable Creative Commons License

Miselis, J. L., & Lorenzo-Trueba, J. (2017). Natural and human-induced variability in barrier-island response to sea level rise. *Geophysical Research Letters*, *44*(23), 11–922. https://doi.org/10.1002/2017GL074811

Morton, R. A., & Payne, J. G. (1985). Beach and vegetation-line changes at Galveston Island, Texas: Erosion, deposition and recovery from hurricane Alicia. In *Geological Circular*, (pp. 85–5). Bureau of Economic Geology.

Morton, R. A., & Sallenger, A. H. (2003). Morphological impacts of extreme storms on sandy beaches and barriers. *Journal of Coastal Research*, *19*, 560–573. Retrieved from https://www.jstor.org/stable/4299198

Mulhern, J. S., Johnson, C. L., & Martin, J. M. (2017). Is barrier island morphology a function of tidal and wave regime? *Marine Geology*, *387*, 74–84. https://doi.org/10.1016/j.margeo.2017.02.016

National Geodetic Survey. (2022). Emergency response imagery. Retrieved from https://storms.ngs.noaa.gov

National Oceanic and Atmospheric Administration (NOAA). (2022). Digital coast data access viewer. Retrieved from https://coast.noaa.gov/dataviewer/%23/

Nienhuis, J. H., Heijkers, L. G. H., & Ruessink, G. (2021). Barrier breaching versus overwash deposition: Predicting the morphologic impact of storms on coastal barriers. *Journal of Geophysical Research: Earth Surface*, *126*(6), e2021JF006066. https://doi.org/10.1029/2021JF006066

Nienhuis, J. H., & Lorenzo-Trueba, J. (2019a). Can barrier islands survive sea-level rise? Quantifying the relative role of tidal inlets and overwash deposition. *Geophysical Research Letters*, *46*(24), 14613–14621. https://doi.org/10.1029/2019GL085524

Nienhuis, J. H., & Lorenzo-Trueba, J. (2019b). Simulating barrier island response to sea level rise with the barrier island and inlet environment (BRIE) model v1.0. *Geoscientific Model Development*, *12*(9), 4013–4030. https://doi.org/10.5194/gmd-12-4013-2019

Nordstrom, K. F. (1994). Beaches and dunes of human-altered coasts. *Progress in Physical Geography*, *18*(4), 497–516. https://doi.org/10.1177/030913339401800402

Nordstrom, K. F. (2004). *Beaches and dunes of developed coasts* (2nd ed.). Cambridge University Press.

Overbeck, J. R., Long, J. W., Stockdon, H. F., & Birchler, J. J. (2015). Enhancing evaluation of post-storm morphologic response using aerial orthoimagery from Hurricane Sandy. In P. Wang & J. D. Rosati (Eds.), *Coastal sediments 2015*. World Scientific. https://doi.org/10.1142/9789814689977_0250

Paola, C., Straub, K., Mohrig, D., & Reinhardt, L. (2009). The "unreasonable effectiveness" of stratigraphic and geomorphic experiments. *Earth-Science Reviews*, *97*(1–4), 1–43. https://doi.org/10.1016/j.earscirev.2009.05.003

Passeri, D. L., Dalyander, P. S., Long, J. W., Mickey, R. C., Jenkins, R. L., Thompson, D. M., et al. (2020). The roles of storminess and sea level rise in decadal barrier island evolution. *Geophysical Research Letters*, *47*(18), e2020GL089370. https://doi.org/10.1029/2020GL089370

Pierce, J. W. (1969). Sediment budget along a barrier island chain. *Sedimentary Geology*, *3*(1), 5–16. https://doi.org/10.1016/0037-0738(69)90012-8

REDcatch GmbH. (2022). Volume calculation tool for QGIS3. Retrieved from https://github.com/REDcatch/Volume_calculation_for_QGIS3

Reeves, I. R. B., Goldstein, E. B., Moore, L. J., & Zinnert, J. C. (2022). Exploring the impacts of shrub-overwash feedbacks in coastal barrier systems with an ecological-morphological model. *Journal of Geophysical Research: Earth Surface*, *127*(3), e2021JF006397. https://doi.org/10.1029/2021JF006397

Rodgers, N., & Paola, C. (2021). Intermittent retreat behavior in experimental barrier island response to constant sea level rise and wave forcing. *Journal of Geophysical Research: Earth Surface*, *126*(8), e2021JF006086. https://doi.org/10.1029/2021JF006086

Rodriguez, A. B., Theuerkauf, E. J., Ridge, J. T., VanDusen, B. M., & Fegley, S. R. (2020). Long-term washover fan accretion on a transgressive barrier island challenges the assumption that paleotempestites represent individual tropical cyclones. *Scientific Reports*, *10*(1), 19755. https://doi.org/10.1038/s41598-020-76521-4

Rogers, L. J., Moore, L. J., Goldstein, E. B., Hein, C. J., Lorenzo-Trueba, J., & Ashton, A. D. (2015). Anthropogenic controls on overwash deposition: Evidence and consequences. *Journal of Geophysical Research: Earth Surface*, *120*(12), 2609–2624. https://doi.org/10.1002/2015JF003634

Sallenger, A. H., Jr. (2000). Storm impact scale for barrier islands. *Journal of Coastal Research*, *16*(3), 890–895. Retrieved from https://www.jstor.org/stable/4300099

Sherwood, C. R., Dongeren, A. V., Doyle, J., Hegermiller, C. A., Hsu, T. J., Kalra, T. S., et al. (2021). Modeling the morphodynamics of coastal responses to extreme events: What shape are we in? *Annual Review of Marine Science*, *14*(1), 457–492. https://doi.org/10.1146/annurev-marine-032221-090215

Sherwood, C. R., Warrick, J. A., Hill, A. D., Ritchie, A. C., Andrews, B. D., & Plant, N. G. (2018). Rapid, remote assessment of Hurricane Matthew impacts using four-dimensional structure-from-motion photogrammetry. *Journal of Coastal Research*, *34*(6), 1303–1316. https://doi.org/10.2112/JCOASTRES-D-18-00016.1

Smallegan, S. M., & Irish, J. L. (2017). Barrier island morphological change by bay-side storm surge. *Journal of Waterway, Port, Coastal, and Ocean Engineering*, *143*(5), 04017025. https://doi.org/10.1061/(ASCE)WW.1943-5460.0000413

Stutz, M. L., & Pilkey, O. H. (2011). Open-ocean barrier islands: Global influence of climatic, oceanographic, and depositional settings. *Journal of Coastal Research*, *27*(2), 207–222. https://doi.org/10.2112/09-1190.1

Tuck, M. E., Ford, M. R., Masselink, G., & Kench, P. S. (2019). Physical modelling of reef island topographic response to rising sea levels. *Geomorphology*, *345*, 106833. https://doi.org/10.1016/j.geomorph.2019.106833

Tuck, M. E., Kench, P. S., Ford, M. R., & Masselink, G. (2019). Physical modelling of the response of reef islands to sea-level rise. *Geology*, *47*(9), 803–806. https://doi.org/10.1130/G46362.1

Velasquez-Montoya, L., Sciaudone, E. J., Smyre, E., & Overton, M. F. (2021). Vulnerability indicators for coastal roadways based on barrier island morphology and shoreline change predictions. *Natural Hazards Review*, *22*(2), 04021003. https://doi.org/10.1061/(ASCE)NH.1527-6996.0000441

Williams, H. E., Lazarus, E. D., & Goldstein, E. B. (2022). Data and morphometric results from a physical experiment simulating washover deposition [Dataset]. Zenodo. https://doi.org/10.5281/zenodo.7075282

Williams, H. F. L. (2015). Contrasting styles of Hurricane Irene washover sedimentation on three east coast barrier islands: Cape lookout, North Carolina; Assateague Island, Virginia; and Fire Island, New York. *Geomorphology*, *231*, 182–192. https://doi.org/10.1016/j.geomorph.2014.11.027

Williams, H. F. L., & Rains, B. J. (2022). Effect of barrier height on magnitude and character of Hurricane Harvey washover fans, Matagorda Peninsula, Texas, USA. *Journal of Coastal Research*, *38*(1), 133–139. https://doi.org/10.2112/JCOASTRES-D-21-00043.1

Williams, J. J., Buscombe, D., Masselink, G., Turner, I. L., & Swinkels, C. (2012). Barrier dynamics experiment (BARDEX): Aims, design and procedures. *Coastal Engineering*, *63*, 3–12. https://doi.org/10.1016/j.coastaleng.2011.12.009

19448007, 2022, 22, Downloaded from https://agupubs.onlinelibrary.wiley.com/doi/10.1029/2022GL100098, Wiley Online Library on [13/11/2023]. See the Terms and Conditions (https://onlinelibrary.wiley.com/terms-and-conditions) on Wiley Online Library for rules of use; OA articles are governed by the applicable Creative Commons License